Applied Energy 183 (2016) 746–759

Contents lists available at ScienceDirect

Applied Energy

journal homepage: www.elsevier.com/locate/apenergy

Analysis of the dynamic characteristics of combustion instabilities in a pre-mixed lean-burn natural gas engine

Li-Ping Yang [a,*], En-Zhe Song [a], Shun-Liang Ding [a], Richard J. Brown [b], Norbert Marwan [c], Xiu-Zhen Ma [a]

[a] Institute of Power and Energy Engineering, Harbin Engineering University, No. 145-1, Nantong Street, Nangang District, Harbin 150001, China
[b] Biofuel Engine Research Facility, Queensland University of Technology, Brisbane, QLD 4001, Australia
[c] Potsdam Institute for Climate Impact Research, Potsdam 14412, Germany

HIGHLIGHTS

- Combustion instabilities in a pre-mixed lean-burn natural gas engine were studied.
- Effect of gas injection timing on the complexity of combustion system was analysed.
- Analysis is based on return map, recurrence plot, recurrence quantification analysis.
- Source of combustion instabilities is identified based on 3-D CFD simulation.

ARTICLE INFO

Article history:
Received 6 July 2016
Received in revised form 9 September 2016
Accepted 12 September 2016

Keywords:
Natural gas engine
Lean-burn
Combustion instabilities
Gas injection timing (GIT)
Recurrence plots (RPs)
Recurrence qualification analysis (RQA)

ABSTRACT

The cyclic combustion instabilities in a pre-mixed lean-burn natural gas engine have been studied. Using non-linear embedding theory, recurrence plots (RPs) and recurrence qualification analysis (RQA), the hidden rhythms and dynamic complexity of a combustion system in high dimensional phase space for each gas injection timing (GIT) have been examined, and the possible source of combustion instabilities has been identified based on 3-D computational fluid dynamics (CFD) simulation. The results reveal that for lower engine load, with the decrease of mixture concentration, the combustion instability and complexity of combustion system become more sensitive to the variation of GITs. Richer mixture and earlier (GIT < 30°CA ATDC) or delayed (GIT > 90°CA ATDC) gas injection will lead to more stable combustion, regular oscillatory and low complexity of combustion system, while leaner mixture together with the medium GITs (from 30 to 90°CA ATDC) easily leads to increase of combustion fluctuations, time irreversibility and dynamic complexity of combustion system. When GITs are changed, the combustion instabilities of pre-mixed lean-burn natural gas engines are from in-cylinder unreasonable stratification of mixture concentration and turbulent motion.

1. Introduction

Energy saving and environmental protection have become two focus issues right around the world, and the development of clean alternative energies in place of petroleum is an effective measure to alleviate these issues. Natural gas is regarded as one of the most promising alternative fuels due to its abundant reserves and clean combustion properties. Reserves of natural gas are 149.76 trillion cubic metres, much larger than for crude oil [1]. The primary constituent of natural gas is methane (CH_4), and it also contains a small amount of heavier hydrocarbons (ethane, propane and butane) and inert gases (carbon dioxide and nitrogen). The hydrogen to carbon ratio (H/C) of natural gas is close to 3.8 and is the highest of all hydrocarbon fuels. Therefore, the combustion of natural gas produces the least CO_2 per unit of energy released for all hydrocarbon fuels [2,3]. For example, natural gas produces 25–30% less CO_2 emissions per unit of energy than gasoline and diesel [4,5]. At the same time, oxides of nitrogen (NOx), sulphur dioxide (SO_2) and particulate matter (PM) emissions produced in the combustion process are lower than for petroleum-based fuels, so natural gas is widely applied as one of the most ideal fuels of internal combustion engines [6,7].

Currently, pre-mixed natural gas engines using multi-point manifold gas injection are being more widely used in the vehicle, marine and power plant fields. In order to meet the increasingly strict emission restrictions and demands for fuel efficiency, lean-burn and exhaust gas recirculation (EGR) technologies are

* Corresponding author.
E-mail address: yangliping302@hrbeu.edu.cn (L.-P. Yang).

http://dx.doi.org/10.1016/j.apenergy.2016.09.037
0306-2619/

considered to be the most effective measures to further improve fuel efficiency and to minimise NOx emissions on natural gas engines [8–11]. However, a mixture of air and gas that is too lean, or an excessive EGR supplied to a cylinder may cause combustion instability [12,13], and cycle-to-cycle variations (CCV) - which are an inherent consequence of combustion instability - leading to poor thermal efficiency and an increase of CO and UHC emissions [14,15]. If CCV can be eliminated, engine power output will increase by 10% for the same fuel consumption in a spark ignition (SI) engine [16]. The effects of some boundary conditions and structure parameters on combustion characteristics and engine performance were estimated [17–21]. However, during the actual operating process of the lean-burn natural gas engine, the apparently stochastic character of CCV makes it difficult to control. Therefore, it is one of the most important issues in the field of internal combustion engines to further understand the internal nature of CCV, to identify their sources and then develop effective engine control strategies for highly efficient combustion [22–29].

The nature of CCV in internal combustion engines has been widely investigated. However, sometimes researchers have reported apparently conflicting observations. For example, some have described CCV as strictly stochastic, while others have illustrated the determinism which has been typically characterised in strictly linear terms [30–32]. Daily has indicated that CCV are an inherent consequence of non-linear combustion kinetics, and that highly chaotic behaviour will occur when the burn time occupies an excessive fraction of the cycle time [33]. Non-linear dynamic theory has been increasingly applied to analyse the dynamic properties of CCV in internal combustion engines because it is a more sophisticated approach to reveal the complexities of such a dynamic system. Litak et al. analysed the noise level of maximum peak pressure fluctuations in a single-cylinder spark ignition (SI) engine by means of coarse-grained entropy and an autocorrelation function, and indicated that the dynamic of the combustion is a non-linear multidimensional process mediated by noise [34]. Curto-Risso et al. used the correlated integral and surrogate data to investigate the complexity of cycle-to-cycle heat release variations in a spark ignition engine, and found that low dimensionality is related to the presence of determinism in heat release fluctuations [35]. Wagner et al. used return maps, Shannon entropy and symbol sequence statistics to analyse cycle-to-cycle combustion dynamics, and observed a transition from stochastic behaviour to noisy non-linear determinism when the equivalence ratio was decreased from stoichiometric to very lean conditions [36]. Daw proposed a physically oriented model to predict the lean combustion instability in SI engines. The model combined both stochastic and non-linear deterministic elements and can be used to simulate the interaction between stochastic, small-scale fluctuations in engine parameters and non-linear deterministic coupling between thousands of engine cycles. The results showed that lean combustion instability should occur as a dynamic period-doubling bifurcation sequence [37]. Sen et al. investigated the complex dynamics of cyclic combustion heat release variations in a spark ignition (SI) engine by multifractal and statistical analyses. The multifractal complexity is based on the singularity spectrum of the heat release time series in terms of the Hölder exponent. The result indicated that the complexity increases with an increasing spark advance angle. The kurtosis of their probability density functions was calculated to perform a statistical analysis of combustion fluctuations [38]. Wavelet analysis also was used to characterise the dynamics of CCV in SI engines [39–41].

Usually, time series of in-cylinder pressure, indicated mean effective pressure (IMEP) or heat release are used to describe the variation rules of combustion systems in internal combustion engines [34–36,38,42–44]. The dynamic state and its evolution process of combustion system attractor in a high dimensional phase space can only be visualised by projection into two or three dimensional subspace. However, the recurrence plot (RP) makes it possible to investigate the dynamic characteristics of the motion trajectory of combustion system attractors in an m-dimensional phase space by using a two-dimensional representation of its recurrences. As a graphical tool, the RP can be used to visualise the recurrences of dynamic systems and to reveal temporal correlations. It can provide a qualitative picture of the correlations between the different states of the combustion system in a natural gas engine. The information contained in RPs is rich and manifold, and often cannot be easily obtained by other methods [45]. Furthermore, recurrence quantitative analysis (RQA) introduced by Zbilut and Webber (and extended by Marwan et al.), can move beyond the visual impression from RPs and provide the quantitative characteristics of the dynamic system [46,47]. Another advantage of RQA is that it can provide useful information even for non-stationary and short data when other analysis methods fail, such as identifying laminar states or detecting transitions between regular or chaotic regimes in complex systems [48–51].

The natural gas engine is a complex dynamic system, and the combustion instabilities in lean-burn SI natural gas engines are determined by a wide variety of factors [52]. Among these factors, only a few parameters can be directly controlled or flexibly modified by the experimenters based on test purpose during engine operation, such as ignition (ignition timing, duration and energy), gas injection (injection timing and quantity) and throttle opening. Gas injection timing (GIT) has a strong influence on mixture formation and the combustion process in natural gas engines [53–57]. From the above literature, it is obvious that the majority of the research work regarding combustion instabilities and dynamic properties of combustion systems has been done on SI engines. But only a few research works in the relevant literature have focused on the effect of GIT on combustion instabilities of pre-mixed lean- burn natural gas engines. No study has been performed to elucidate the effects of GIT on dynamic complexity of the combustion process in pre-mixed lean-burn natural gas engines.

In this regard, the main objectives of the present research are to (i) to investigate the effect of GIT on the combustion instabilities in pre-mixed lean-burn natural gas engines, (ii) to reveal temporal correlations, and quantitatively and qualitatively analyse the hidden rhythms and the dynamic complexity of the combustion system using chaos theory and more sophisticated non-linear data analysis methods (including return map, RPs and RQA), and (iii) to identify the possible sources of combustion instabilities when GIT is changed, based on 3-D computational fluid dynamics (CFD) calculations. Our research results are useful to understand the complex dynamics of cyclic combustion instabilities and may provide useful information to improve control strategies for gas fuel injection leading to improvements in the performance of pre-mixed lean-burn natural gas engines.

2. Facilities and experiment

Tests were conducted on a modified single cylinder, water-cooled, intake port injection natural gas engine. The test dynamometer used in our study is an eddy current dynamometer with an automatic control function. It can work in constant speed control and constant torque control modes. During the experiment process, all other feedback controls were cancelled except for engine speed. Air-to-fuel ratio and gas mass flow rate were real-time monitored using a Lambda meter and gas flow meter respectively. The in-cylinder pressure data, crank angle and top dead centre (TDC) signals were captured by a high-speed data acquisition system which includes a cylinder pressure sensor, a

charge amplifier, a crank angle encoder, a 621 combustion analyser and a computer. The testing apparatus are shown in Table 1. The cylinder pressure sensor, which is a piezoelectric sensor, was mounted on the engine cylinder head, which can provide direct measurement data of the combustion pressure in-cylinder. The highest sampling resolution of the data acquisition system was 0.1 degrees of crankshaft angle (°CA). In our experiment, a sampling resolution of 1°CA was chosen because it has sufficient accuracy to describe each combustion process of a natural gas engine. The cylinder pressure data file of a single test contained 1800 cycles of engine work. A schematic of the experimental bench is presented in Fig. 1.

In order to comprehensively test the effect of GIT on combustion instabilities of lean-burn natural gas engines, the engine experiment was conducted at the whole range of engine speeds and loads, the engine speed being from 800 to 1400 rpm (with the corresponding crankshaft frequency being from 13.3 to 23.3 Hz), and the engine load rate being from 0 to 100% at each engine speed.

At each engine load rate, excess air coefficient λ was increased from 1 to the lean flammable limit of the natural gas engine. This lean limit means that when λ approaches or reaches a certain value, the engine is hardly controlled, and drastic fluctuations of power output or engine stalling will occur. For each engine load and speed, pause width of gas injection was kept constant, so λ (excess air coefficient) was fixed, and GIT was varied within the effective intake valve opening duration. Every interval of GIT is 30°CA. Fig. 2 illustrates the curves of intake and exhaust valve lift, as well as gas injection control signals when λ is 1.4 with the engine operating at a load rate of 10% and engine speed of 1000 rpm. GIT is from 1 to 150°CA after top dead centre (ATDC) of the intake stroke.

3. Non-linear time series analysis methods

The Indicated Mean Effective Pressure (IMEP) of all engine testing cycles (1800 cycles) was calculated based on in-cylinder pressure and cylinder volume. These data have then been analysed by visual inspection of the phase space and the corresponding RPs as well as quantitatively by RQA.

3.1. Phase space reconstruction

Phase space reconstruction is a useful way to reconstruct the attractor of a dynamic system based on a limited time series $x(i)$, ($i = 1, 2, \ldots, N$) and to investigate the system's dynamics. The reconstruction procedure is based on a time-delay embedding providing a set of m-dimensional vectors:

$$\mathbf{X}_i = \{x(i), x(i+\tau), \ldots, x(i+(m-1)\tau\} \quad i = 1, 2, \ldots, N-(m-1)\tau \tag{1}$$

where $x(i)$ is the IMEP time series, $\mathbf{X}_i$ is the corresponding phase space vector, N is the total sampling number, m is the embedding dimension, and τ is the time delay. m and τ are crucial parameters for the reconstruction of the phase space and must be selected properly, e.g. with the help of a sophisticated algorithm. If m is set too small, the dynamic system will be under-determined and false recurrences can occur. If m is selected too large, a significant amount of artefacts can appear [48]. If the chosen τ is too small or too large, the reconstructed attractor of the dynamic system cannot be sufficiently unfolded. In this study, the mutual information function method [58] and the false nearest neighbours algorithm [59] were used to determine the optimum τ and m respectively.

Table 1
Experimental apparatus.

Facilities	Type	Supplier
Dynamometer	GW160	XIANGYI
Cylinder pressure sensor	GU21	AVL
Crank angle encoder	365C	AVL
Charge amplifier	6125C	KISTLER
Combustion analyser	621	AVL
Gas flow meter	CMF010	EMERSON
Lambda meter	LA4	ETAS

3.2. Recurrence plot (RP)

The RP can be formally expressed by a matrix [35].

An RP is defined as:

$$R_{i,j} = \Theta(\varepsilon - \|\mathbf{X}_i - \mathbf{X}_j\|) \tag{2}$$

where $\mathbf{X}_i$ and $\mathbf{X}_j$ are i-th and j-th points of the state space trajectory, $\|\cdot\|$ is the Euclidean norm, ε is the recurrence threshold and $\Theta(s)$ is the Heaviside function which is defined as:

$$\Theta(s) = \begin{cases} 1 & s \geqslant 0 \\ 0 & s < 0 \end{cases} \tag{3}$$

Hence, the RP is a symmetric and square array of 1 s and 0 s. Entries of 1 represent those pairs of states (points at the reconstructed phase space trajectory) that have distances smaller than the recurrence threshold ε and are considered as recurrences. RPs are usually displayed using the colour black for the value 1.

The threshold ε is a crucial parameter for calculating the RP of a dynamic system. Depending on the application, different rules for its selection have been proposed [49]. Here a criterion was used to ensure a constant density of recurrence points (i.e., recurrence rate, see below).

An RP exhibits characteristic small- and large-scale patterns which are caused by typical dynamic behaviour. For an autonomous or stationary dynamic system such as white noise, the recurrence points in the RP are uniformly distributed [45]. The RPs of periodic and quasi-periodic dynamics consist of periodically occurring continuous diagonal lines or patterns. A paling towards the corners in the RP is caused by systems with slowly varying parameters, e.g. non-stationary systems or trends. Abrupt changes in the dynamics as well as extreme events are characterised by white areas or bands.

The small-scale patterns, such as diagonal and vertical lines, are the base for a recurrence quantification analysis. For example, a diagonal line represents periods of similar evolution of the system. The length of such a line is, therefore, related to the divergence behaviour of the dynamics (and indirectly related to the Lyapunov exponent). Vertical or horizontal lines signify the presence of laminarity or intermittency in the time series [49]. If only single isolated points occur in an RP, the process may be an uncorrelated random or even anti-correlated process.

3.3. Recurrence quantification analysis (RQA)

Several RQA measures have been introduced, most being based on diagonal and vertical lines in the RP [46,47,49]. In our study we focus on the recurrence rate (RR), determinism (DET), divergence (DIV), line length entropy (ENTR), and laminarity (LAM).

The recurrence rate (RR) is a measure quantifying the recurrence density of an RP,

$$RR = \frac{1}{N^2}\sum_{i,j=1}^{N} R_{i,j} \tag{4}$$

It is an estimation of the recurrence probability of the system.

The determinism (DET)

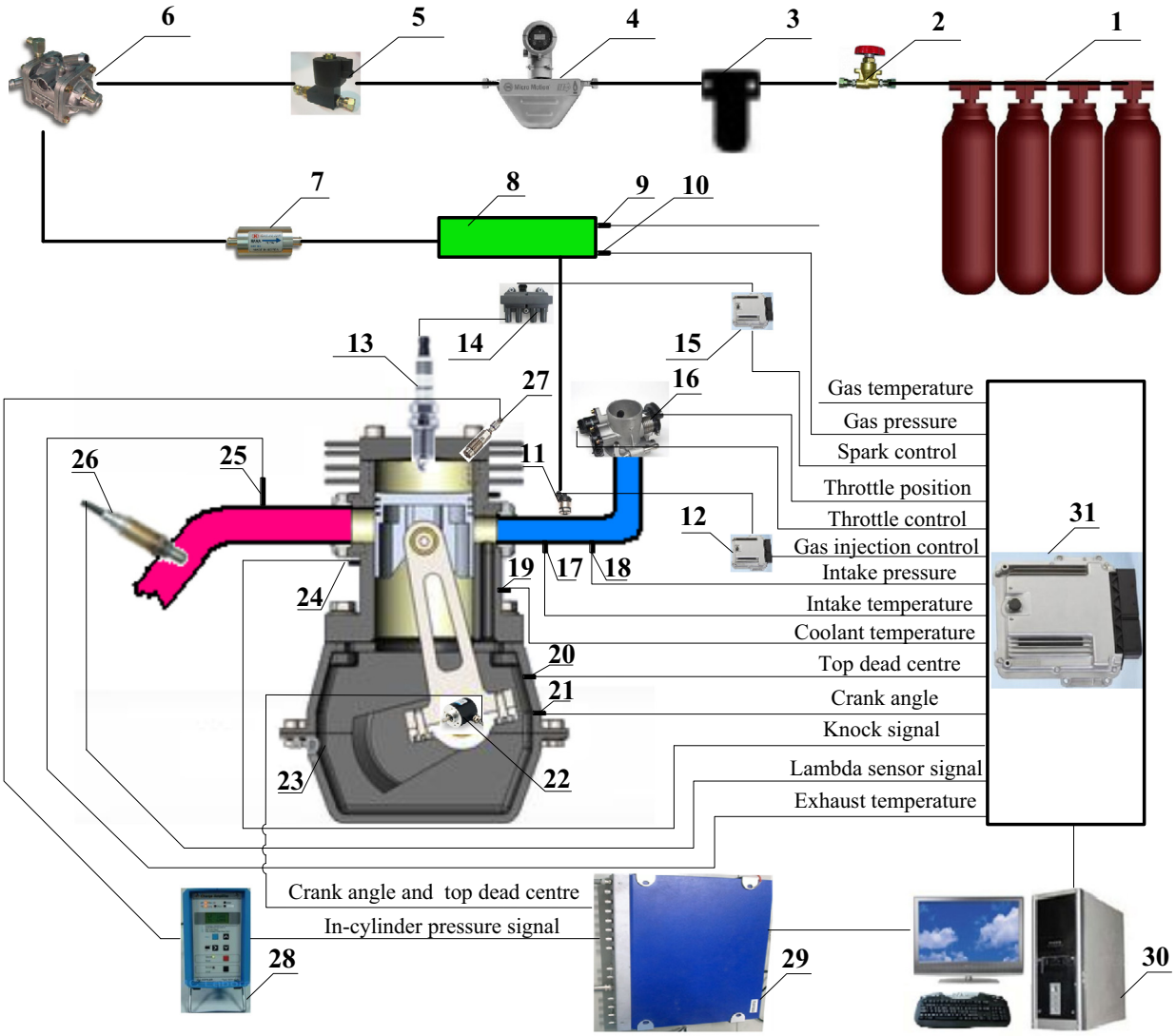

1-natural gas tanks, 2-manual valve, 3-high pressure gas filter, 4-gas flow meter, 5-shut off valve, 6-pressure regulator, 7 low pressure gas filter, 8-gas rail, 9-gas pressure sensor, 10-gas temperature sensor, 11-gas injector, 12-gas injection control module, 13-spark plug, 14-ignition coil, 15- ignition control module, 16-throttle, 17-intake temperature sensor, 18-intake pressure sensor, 19- coolant water temperature sensor, 20- top dead centre (TDC) sensor, 21-crank angle sensor, 22-crank angle encoder, 23-natural gas engine, 24-knock sensor, 25-exhuast temperature sensor, 26-Lambda sensor, 27-cylinder pressure sensor, 28-charge amplifier, 29-combustion analyser, 30-computer, 31- data acquisition and control system

Fig. 1. Schematic of experimental bench. 1-natural gas tanks, 2-manual valve, 3-high pressure gas filter, 4-gas flow meter, 5-shut off valve, 6-pressure regulator, 7 low pressure gas filter, 8-gas rail, 9-gas pressure sensor, 10-gas temperature sensor, 11-gas injector, 12-gas injection control module, 13-spark plug, 14-ignition coil, 15-ignition control module, 16-throttle, 17-intake temperature sensor, 18-intake pressure sensor, 19-coolant water temperature sensor, 20-top dead centre (TDC) sensor, 21-crank angle sensor, 22-crank angle encoder, 23-natural gas engine, 24-knock sensor, 25-exhuast temperature sensor, 26-Lambda sensor, 27-cylinder pressure sensor, 28-charge amplifier, 29-combustion analyser, 30-computer, 31-data acquisition and control system.

$$DET = \frac{\sum_{l=2}^{N} lP(l)}{\sum_{ij}^{N} R_{ij}} \tag{5}$$

is the proportion of recurrence points forming diagonal structures to all recurrent points in the RP ($P(l)$ is the histogram of the line lengths of the diagonal lines). RPs of highly deterministic systems contain mainly diagonal lines, whereas RPs of stochastic systems consist mainly of single dots. Therefore, DET gives some indication about the nature of the dynamics (deterministic vs. random). Hence, this measure in terms of predictability (such as small values indicate low predictability and high values indicate good predictability) can be interpreted.

The longest diagonal line segment excluding the main diagonal line in the RP is indirectly related to the Lyapunov exponent of the dynamics [49]. The inverse of the length of the longest line L_{max} is the RQA measure divergence (DIV).

The measure ENTR refers to the Shannon entropy with respect to the probability $p(l)$ of finding a diagonal line of exactly length l in RP, where

$$p(l) = \frac{P(l)}{\sum_{l=l_{min}}^{N} P(l)}$$

and

$$ENTR = -\sum_{l=l_{min}}^{N} p(l) \ln p(l) \tag{6}$$

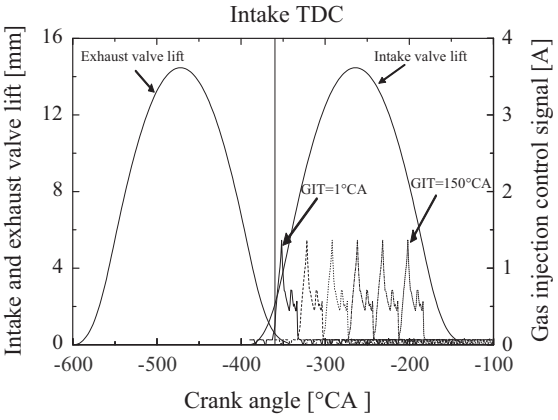

Fig. 2. Curve of intake and exhaust valve lift, as well as the gas injection control signal when engine operates at load rate of 10%, engine speed of 1000 rpm, λ = 1.4.

ENTR is a measure of complexity of the deterministic structure in the examined dynamic system. For example, for uncorrelated noise ENTR has very low values, indicating the low complex nature of the dynamics, whereas for chaotic systems (where the RP contains diagonal lines of different lengths and also single dots) the ENTR is large.

Laminarity (LAM)

$$LAM = \frac{\sum_{v=2}^{N} vP(v)}{\sum_{v=1}^{N} vP(v)} \tag{7}$$

(with $P(v)$ the histogram of vertical line lengths) is analogous to DET, but quantifying the percentage of recurrent points forming the vertical lines rather than diagonal line structures. This measure can be used to indicate the extent of laminar phases or intermittency in the studied system [51].

4. Results and discussion

After comparing the effect of GIT on the combustion instabilities of the lean-burn natural gas engine at different engine speed, load and λ, we can observe that the combustion instabilities of the natural gas engine are more sensitive to the variation of GIT at lower load and leaner mixture. Figs. 3–6 show the time series of IMEP when λ is 1.4 and 1.6, the engine load is 25% and 10%, and engine speed is 1000 rpm.

We can see that as the mixture concentration becomes leaner, the engine cyclic combustion fluctuations increase. However, an optimised GIT can improve the combustion stabilities and further extend the effective lean-burn boundary of pre-mixed natural gas engines. For instance, when the engine operates at a load rate of 25% and λ is 1.4, the minimum co-efficient of cyclic combustion variation based on the IMEP (COV_{IMEP}) is 1.7%, which occurs at GIT of 30°CA ATDC. However in Fig. 4, when the engine operates at a load rate of 25% and λ is 1.6, the maximum coefficient of cyclic combustion variation is 6.1%, which occurs at GIT of 1°CA ATDC. A more steady combustion occurs after GIT of 90°CA ATDC, and the minimum COV_{IMEP} is only 2.0% when GIT is 120°CA ATDC.

Compared to the engine load rate of 25%, the combustion instabilities of the natural gas engine at an engine load rate of 10% are more sensitive to the variations of GIT, with the combustion process being more complex. Figs. 5 and 6 indicate the IMEP time series, when the engine operates at a load rate of 10% and engine speed of 1000 rpm. For the engine load of 10%, the pulse width of gas fuel injection is only 32°CA. The fuel injection occupies a shorter cycle time of intake stroke when compared to the effective open period of the intake valve (228°CA), which allows

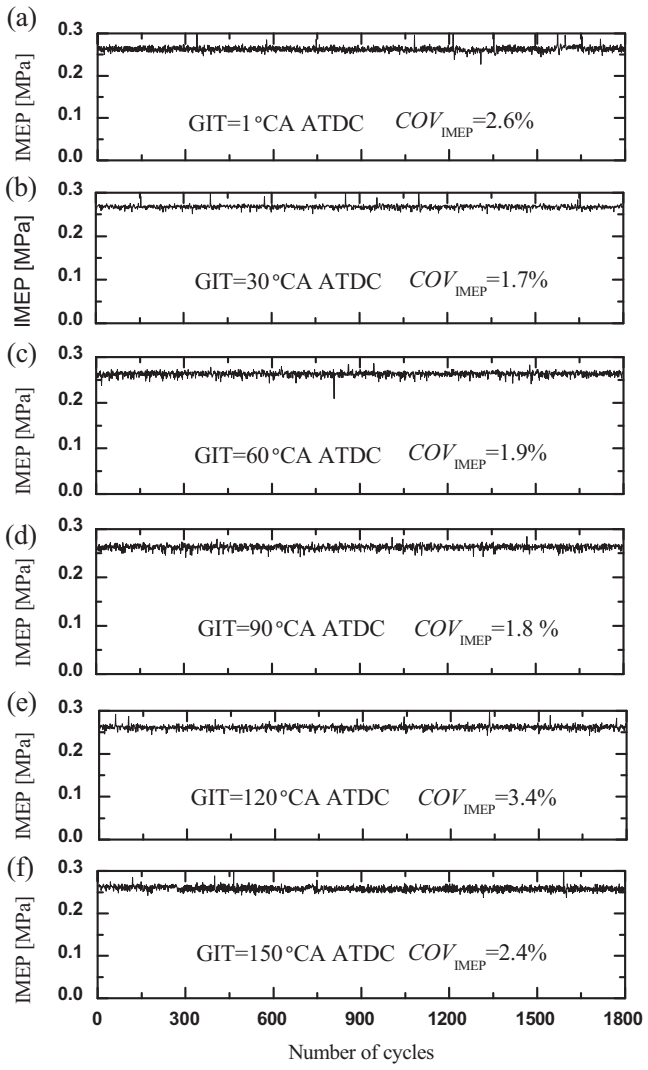

Fig. 3. IMEP time series when λ is 1.4, the engine load rate is 25%, and the engine speed is 1000 rpm.

a wide-range adjustment of GIT, being from 1 to 150°CA ATDC. The minimum GIT of 1°CA ATDC is chosen because it can avoid gas fuel loss caused by scavenging. At that time the pressure is higher than the mixture pressure in the intake port. In order to reduce the effect of possible residual gas fuel in the intake port, the injection direction of gas fuel is designed to be the same as the direction of air flow in the intake pipe, so the kinetic energy of gas fuel can be utilised to speed up the suction of gas fuel.

Fig. 5 depicts IMEP time series exhibiting small-scale fluctuations when natural gas is injected into the intake port during the earlier (before 30°CA ATDC) or later stage (after 90°CA ATDC) of intake stroke, and COV_{IMEP} is no more than 5% for GIT of 1, 90, 120 and 150°CA ATDC. When the GIT is less than 60°CA ATDC, the combustion fluctuations rapidly increase with the increase of GIT, (especially when GIT is 60°CA ATDC), COV_{IMEP} reaches 26%, the engine is difficult to control, and the power output of the lean-burn natural gas engine decreases rapidly. With the decrease of mixture concentration, the effect of GIT on combustion instabilities becomes increasingly obvious (see Fig. 6), especially if natural gas is injected into the intake port near 60°CA ATDC. Partial combustion and misfire frequently occur, leading to engine stalling (see Fig. 6(c)). This phenomenon in Figs. 5 and 6 clearly reveals the potential to further improve engine fuel efficiency and reduce

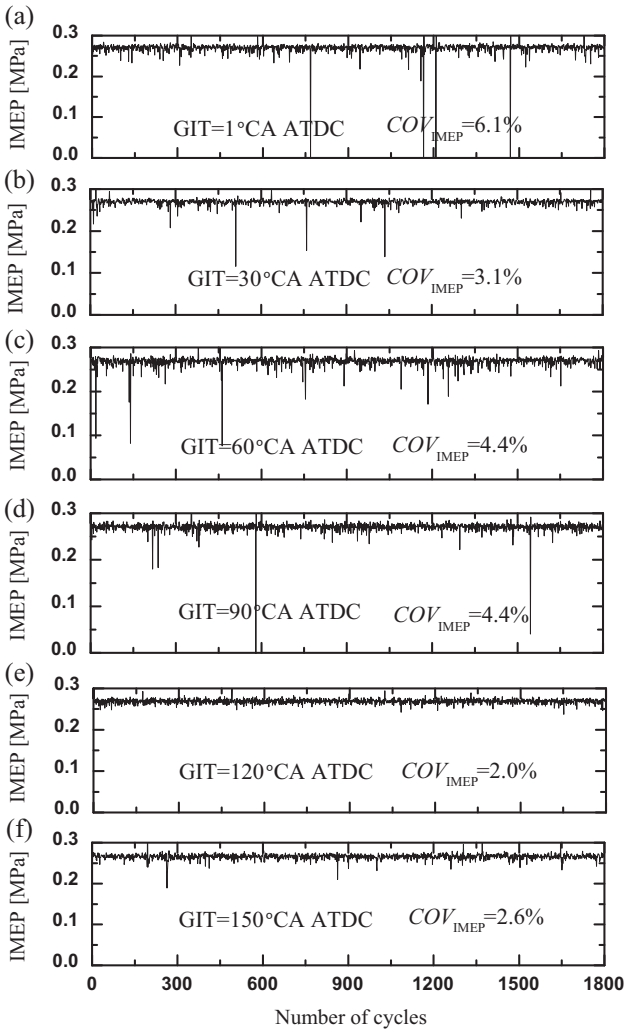

Fig. 4. IMEP time series when λ is 1.6, the engine load rate is 25%, and the engine speed is 1000 rpm.

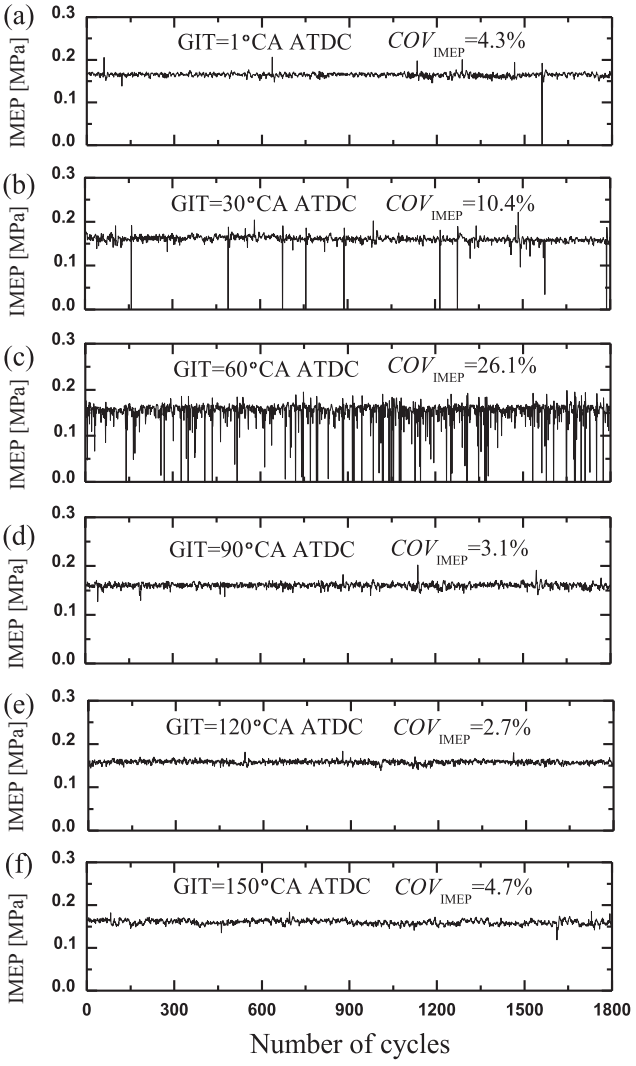

Fig. 5. The IMEP time series when λ is 1.4, the engine load is 10%, and the engine speed is 1000 rpm.

NOx emissions as well as extending the lean-burn limit of natural gas engines by optimising the GIT.

Based on the complexity of the combustion process under lower engine load and leaner mixture, in the following sections of this paper a phase space reconstruction will be performed, plot RPs and the measures of RQA will be calculated when the engine load rate is 10%, λ is 1.4 and 1.6, and GIT was varied from 1 to 150°CA ATDC.

In this study, the mutual information function method was used to determine the optimal time delay τ, accompanied with the visualisation of the attractor structure in the phase space. We used the false nearest neighbours method to determine the optimum embedding dimension of IMEP time series and the recurrence threshold ε was chosen to ensure a constant recurrence rate of RR = 0.1. The selected values of m, τ and ε are shown in Table 2.

The mean (μ) and standard deviation (σ) of the IMEPs were calculated when the engine load rate is 10%, engine speed is 1000 rpm, λ is 1.4 and 1.6, and GIT is from 1 to 150°CA ATDC (see Fig. 7). Fig. 7 shows that for λ = 1.4 and λ = 1.6, as mixture concentration becomes leaner, μ decreases and σ increases, this means that engine effective power output decreases and cyclic combustion stabilities become poor. The minimum of μ and the maximum σ occur at GIT of 60°CA ATDC.

The change of GIT also has a significant effect on the geometric structure of combustion system attractors. Figs. 8 and 9 depict the plots of the two-dimensional phase space reconstruction of IMEP time series when λ is 1.4 and 1.6 respectively, the engine load is 10% and the engine speed is 1000 rpm. The resulting pattern reveals the relationship between the IMEPs for successive cycles. When the earlier or delayed gas injection was used, the patterns of phase space reconstruction possess a quasi-circular structure and appear symmetric about the diagonal which corresponds to the time reversibility, and the distribution region of state points is relatively small; the few state points located away from the centre of the attractor on the phase space are caused by occasional misfires and partial-combustion (see Fig. 8(a), (d), (e) and (f)). However, for some intermediate values of GIT we can see that the distribution of state points on the phase space exhibits a strong randomness, which leads to the small mean and larger standard deviation of IMEPs corresponding to the deterioration of the combustion stability as shown in Fig. 8(b) and (c). The combustion system attractor has a loosened and bifurcated geometry structure; the bifurcation parts of the attractor were described as "characteristic arms" in [60].

As the engine is operated near the lean-burn limit, the combustion stabilities become even poorer, the mean of IMEPs decreases and the standard deviation increases when compared with use of the richer mixture, and the patterns of combustion system

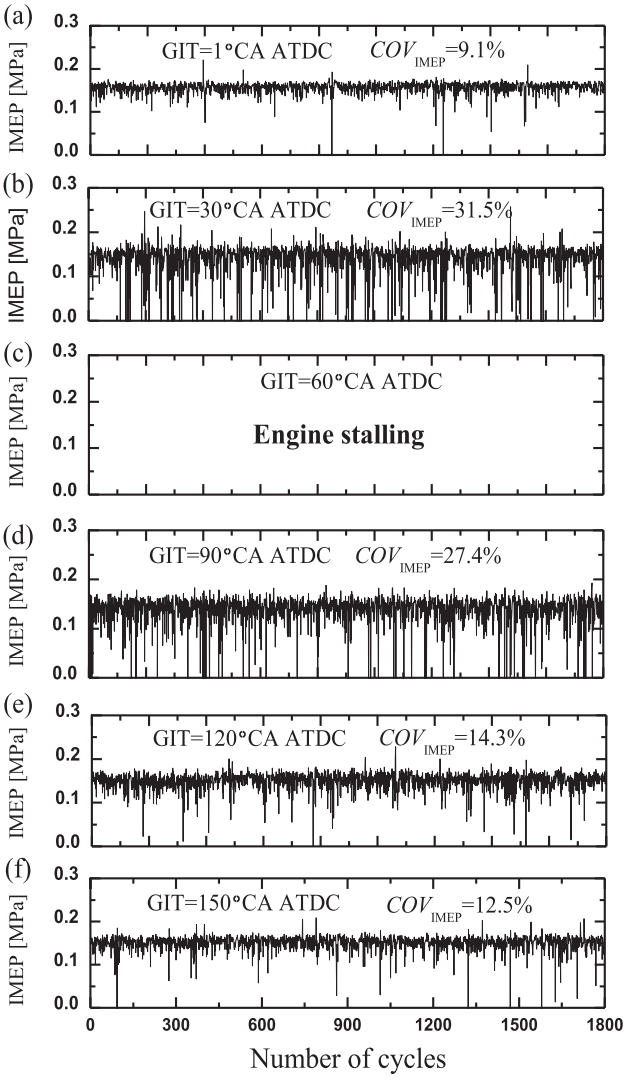

Fig. 6. The IMEP time series when λ is 1.6, the engine load rate is 10%, and the engine speed is 1000 rpm.

attractors described in Fig. 9 are very different from the attractor structure described in Fig. 8. For all GITs, the main body of the attractor appears as a triangle, and the "characteristic arm" structures can be clearly observed. The difference between phase space reconstruction plots for each of the GITs in Fig. 9 is that for GIT being from 30 to 90°CA ATDC, the plots of phase space reconstruction exhibit increased asymmetry about the diagonal, the time irreversibility is more obvious, the amount of state points away from the main body of the attractors increases, and the "characteristic arms" become denser as shown in Fig. 9(b) and (d). This leads to engine stalling (see Fig. 9(c)), meaning that a pattern cannot be displayed.

Based on the relationship between the structures in the RPs and the specific dynamic behaviour, the dynamics of the combustion system of lean-burn natural gas engines can be identified. In order to gain insight into the overall impression and the internal textures of RPs, the RPs at different engine operating conditions and their small-scale structures were illustrated. Fig. 10 illustrates the RPs obtained from the IMEP time series, including all work cycles for different GITs when the engine load is 10%, the engine speed is 1000 rpm, and λ is 1.4. Fig. 11 reveals the small-scale structures of Fig. 10. We can observe from Figs. 10 and 11 that there are diagonals, vertical or horizontal lines and white stripes or bands. However, the scale and texture in the RPs are different. For the richer mixture (λ is 1.4), if earlier or delayed injection was used, we can easily find series of short lines parallel to the main diagonal line in the RPs (see Fig. 11(a), (b) and (d)), and a relatively regular checkerboard structure can be observed in Figs. 10(e) and 11(e). Such texture characteristics mean a more regular oscillatory behaviour and a stable combustion process of the combustion system. For GIT of 150°CA ATDC, the RP in Fig. 10(f) has a richer texture, indicating the existence of determinism in the system. Normally, at the engine operating conditions listed above, more stable combustion and higher fuel efficiency can be obtained. However, for GIT of 60°CA ATDC, the RP has a preponderance of vertical or horizontal lines (see Figs. 10(c) and 11(c)), which signifies the presence of laminar states or intermittency in the IMEP time series, which correspond to more drastic combustion fluctuations and reduced power output, as well as poor emission characteristics in pre-mixed lean-burn natural gas engines. In addition, from Fig. 10, it is obvious that several wider white horizontal and vertical bands occur, which may be caused by an occasional misfire or partial combustion. From reconstruction of the phase space, the state points which are far from the main body (see Fig. 8) can be clearly found.

As the mixture concentration becomes leaner, the combustion instabilities increase rather obviously. The structures of the RPs are very different when contrasting Figs. 10 and 12. The latter illustrates the RPs obtained from experimental IMEP time series for different GITs when the engine load is 10%, the engine speed is 1000 rpm, and λ is 1.6. In Fig. 12, the RPs have a preponderance of vertical or horizontal lines. On the whole, the structures are more similar to Fig. 10(c). However, we can see from the small-scale texture of RPs in Fig. 13 that for GIT of 1, 120 and 150°CA ATDC, there are a series of shorter diagonals parallel to the main diagonal (see Fig. 13(a), (e) and (f)). The structures in RPs when GIT is from 30 to 90°CA ATDC (see Fig. 13(b) and (d)) are similar to Fig. 11(c), when more vertical or horizontal lines appear. Although the RP when GIT is 60°CA ATDC cannot be obtained because the severe combustion instabilities led to engine stalling, its structure of RP is predictable based on the above analysis, which should be also similar to Fig. 13(b) and (d). In order to further corroborate the above results and quantitatively analyse the effect of

Table 2
Values of m, τ and ε used for RQA.

GIT	λ = 1.4			λ = 1.6		
°CA ATDC	m	τ	ε	m	τ	ε
1	7	1	0.0046	7	1	0.0150
30	8	1	0.0034	9	1	0.0403
60	10	1	0.0046		–	–
90	8	1	0.0097	10	1	0.0394
120	6	1	0.0094	7	1	0.0196
150	5	1	0.0074	8	1	0.0208

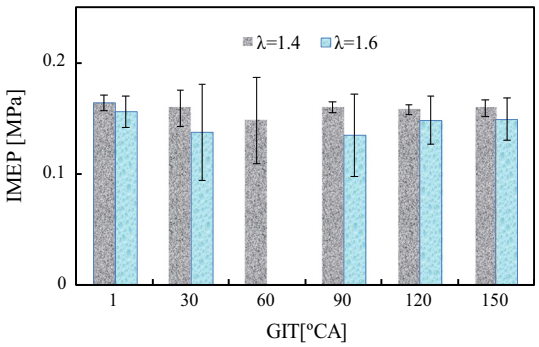

Fig. 7. Statistical analysis results.

GIT on combustion instabilities of lean-burn natural gas engines, RQA was performed in the following analysis.

Using RP, we can qualitatively describe the dynamics of a time series, while RQA allows us to further characterise the dynamics by quantitative measures. In this study, RR, DET, DIV, ENTR, and LAM were analysed for each IMEP time series to identify the complexity of the combustion system and the effect of GIT on combustion instabilities of natural gas engines. The calculation results of the RQA measures can be compared to each other because the same RR parameter (RR = 0.1) was adopted in this study. Fig. 14 presents the calculation results of RQA measures when the engine load rate is 10%, the engine speed is 1000 rpm, λ is 1.4 and 1.6, and GIT is from 1 to 150°CA ATDC. From Fig. 14, the obvious variation rules of RQA measures can be observed when the GIT is changed. DETs are presented in Fig. 14(a) - it shows that the DETs are relatively high for all parameter settings, which are higher than 0.89. When the mixture concentration is held constant, along with the increase of GIT, the values of *DET* slightly increase first, and then decrease; *DET* is highest at GIT of 60°CA ATDC. For different mixture concentrations, the values of *DET* are higher using leaner mixture except for a GIT of 1°CA ATDC, but the variations of *DET* are quite small. This may indicate the good predictability of the combustion system in lean-burn natural gas engine under different engine operating conditions. The behaviours of DIV versus GIT are presented in Fig. 14(b). Along with increase of GIT, DIV decreases first, and then increases for constant mixture concentration. The minimum value of DIV occurs at GIT of 60°CA ATDC, which is equal to 0.162 when λ = 1.4. Comparing to leaner mixture, the DIVs are higher for different GITs (except for 1°CA ATDC) using richer mixture. In Fig. 14(c), for a different concentration mixture, a similar variation tendency of the measure LAM versus GIT was observed. Namely, with the increase of GIT, LAM will increase first, and then decrease, with the peak of LAM occurring at 60°CA ATDC. This means that the extent of laminar phases or intermittency in the IMEP time series increases, which can further validate our analysis related to Figs. 11 and 13. However, for different mixtures, there is not an obvious variation rule of LAM at the same GITs. ENTRs for every GIT under different concentration mixtures are plotted in Fig. 14(d). Note that for a constant mixture concentration, as GIT increases, the values of ENTR increase first, and then decrease. ENTR also reaches its local maximum at GIT of 60°CA ATDC, and except for GIT of 1 and 30°CA ATDC, ENTRs are higher for leaner mixture. The more complex the deterministic structure, the larger the ENTR value, so we can conclude that a non-optimised GIT and a too-lean mixture will lead to an increase in the combustion instabilities and complexity of the combustion system in lean-burn natural gas engines.

In order to further gain insight into the source of combustion instabilities and to explain the complex dynamics of combustion systems in lean-burn natural gas engines, the distribution of CH_4 concentration in-cylinder was also visualised by the 3-D CFD numerical simulation method. Figs. 15 and 16 illustrate the distribution of in-cylinder CH_4 and OH concentration distributions when the engine speed is 1000 rpm, engine load rate is 10%, λ is 1.6 and GIT is from 1 to 120°CA ATDC. The ignition timing is 30°CA before compression TDC, the axial cross sections across the centre of the spark plug were selected when the engine piston is located at 32°CA before compression TDC. The engine load of 10% and λ of 1.6 were chosen to simulate the CH_4 concentration field because the combustion instabilities of natural gas engines are more

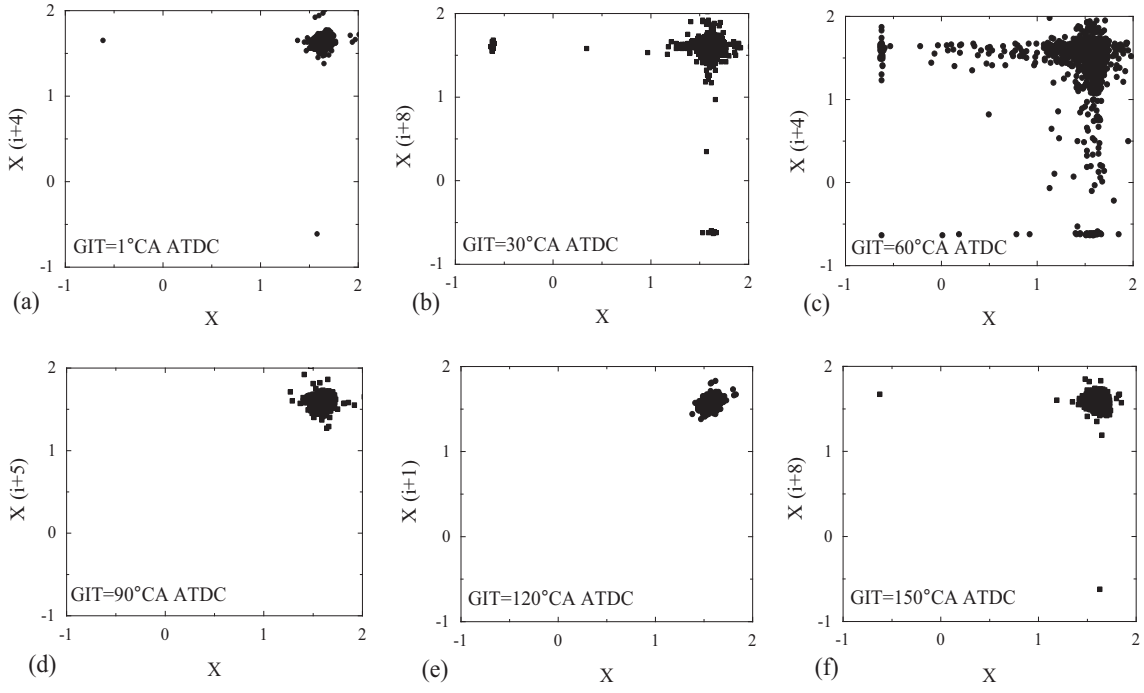

Fig. 8. Plots of phase space reconstruction of IMEP time series when λ = 1.4, the engine load is 10% and the engine speed is 1000 rpm.

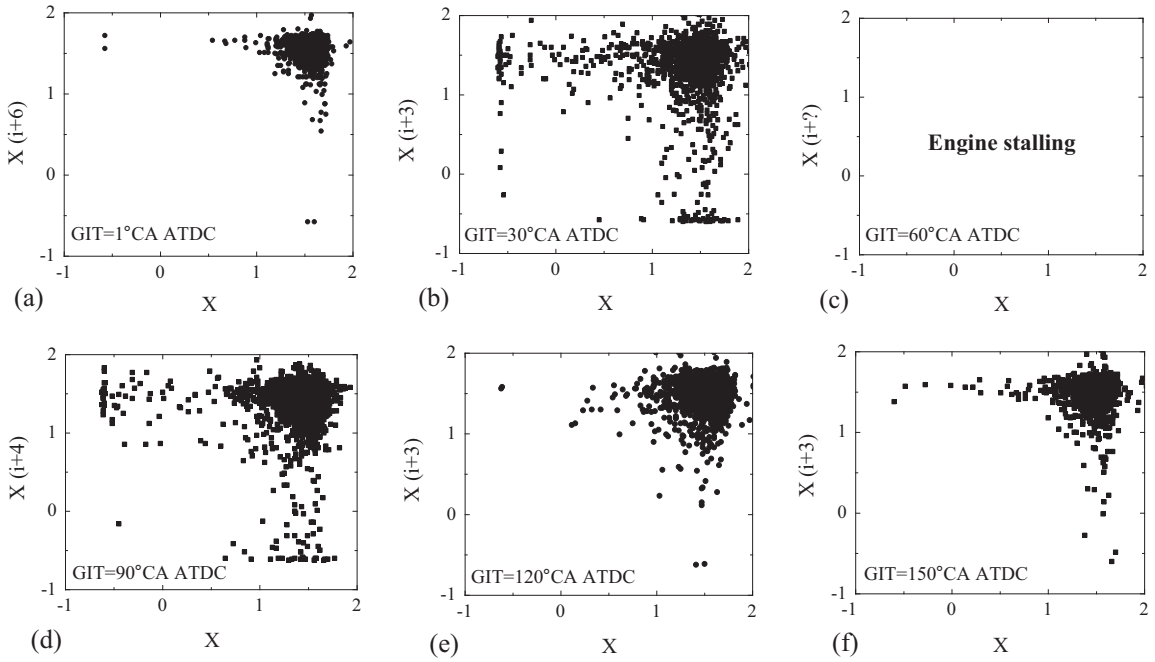

Fig. 9. Plots of phase space reconstruction of IMEP time series when $\lambda = 1.6$, the engine load is 10% and the engine speed is 1000 rpm.

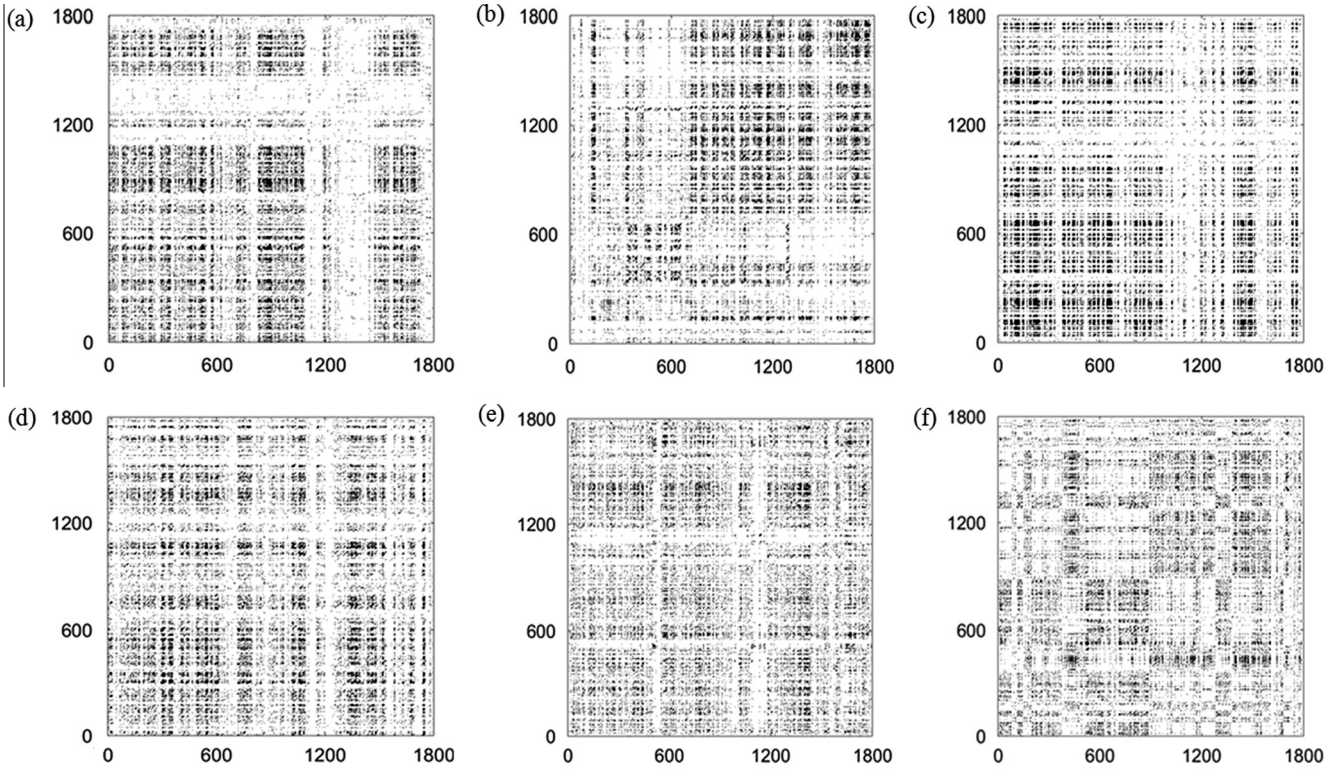

Fig. 10. RPs when $\lambda = 1.4$, the engine load is 10% and the engine speed is 1000 rpm: (a–f) correspond to GITs of 1, 30, 60, 90, 120 and 150°CA ATDC.

sensitive to variation in GIT, and their combustion system is more complex. We also sought to determine why engine stalling occurs at GIT of 60°CA ATDC. The distribution of CH_4 when GIT is 150°CA ATDC is not given here because we observed the fuel gas residual in the intake port during simulation process - although in theory there is enough time before the intake valve closes – and gas fuel can be drawn into the cylinder. In fact the flow speed of the mixture of gas fuel and air in the intake port is quite low, because when the engine load rate is 10%, the opening of the throttle is only 7.2°, after air goes through the small gap between the inner wall and the valve plate of the throttle, the air expands, the pressure increases and flow speed decreases rapidly. Perhaps this can help us to understand why the textures of RP in Figs. 10(f) and 11(f) are different from other conditions. These differences may be

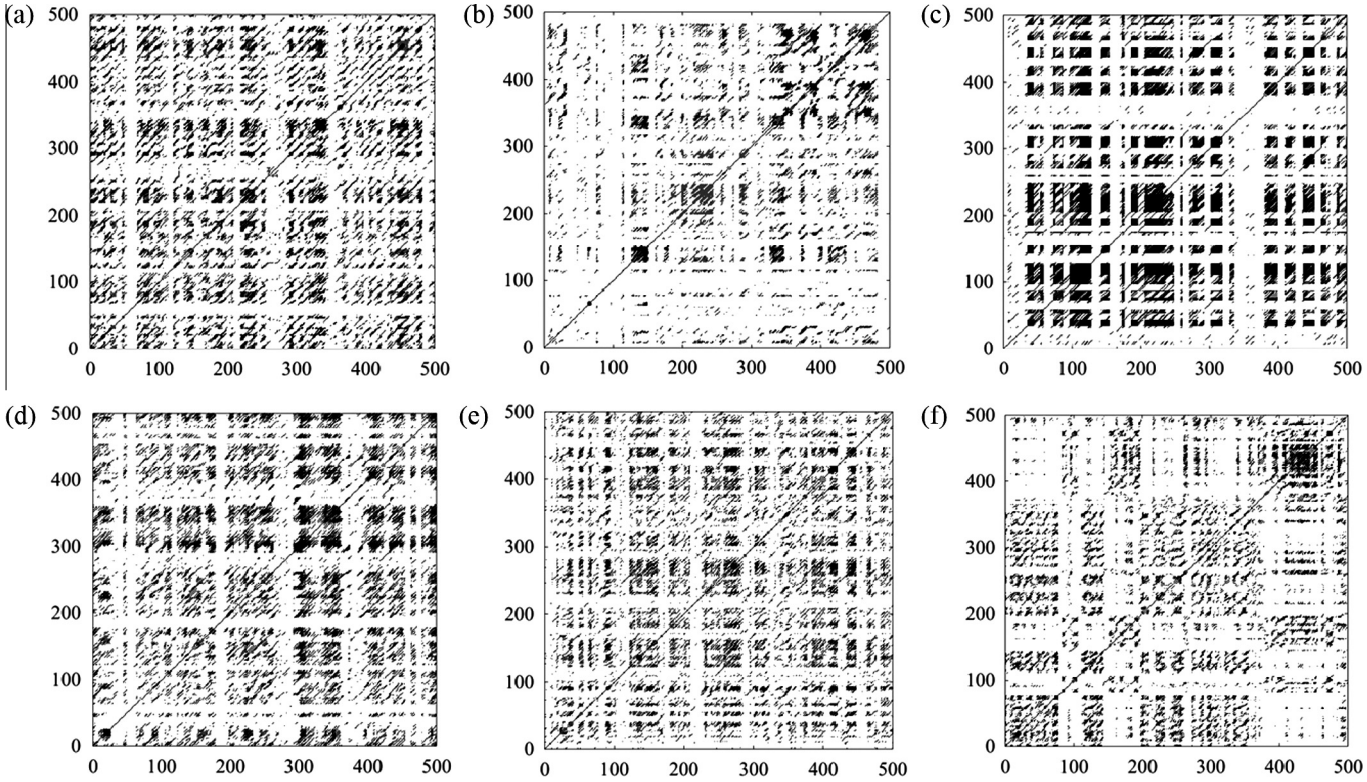

Fig. 11. The small-scale structures of Fig. 10.

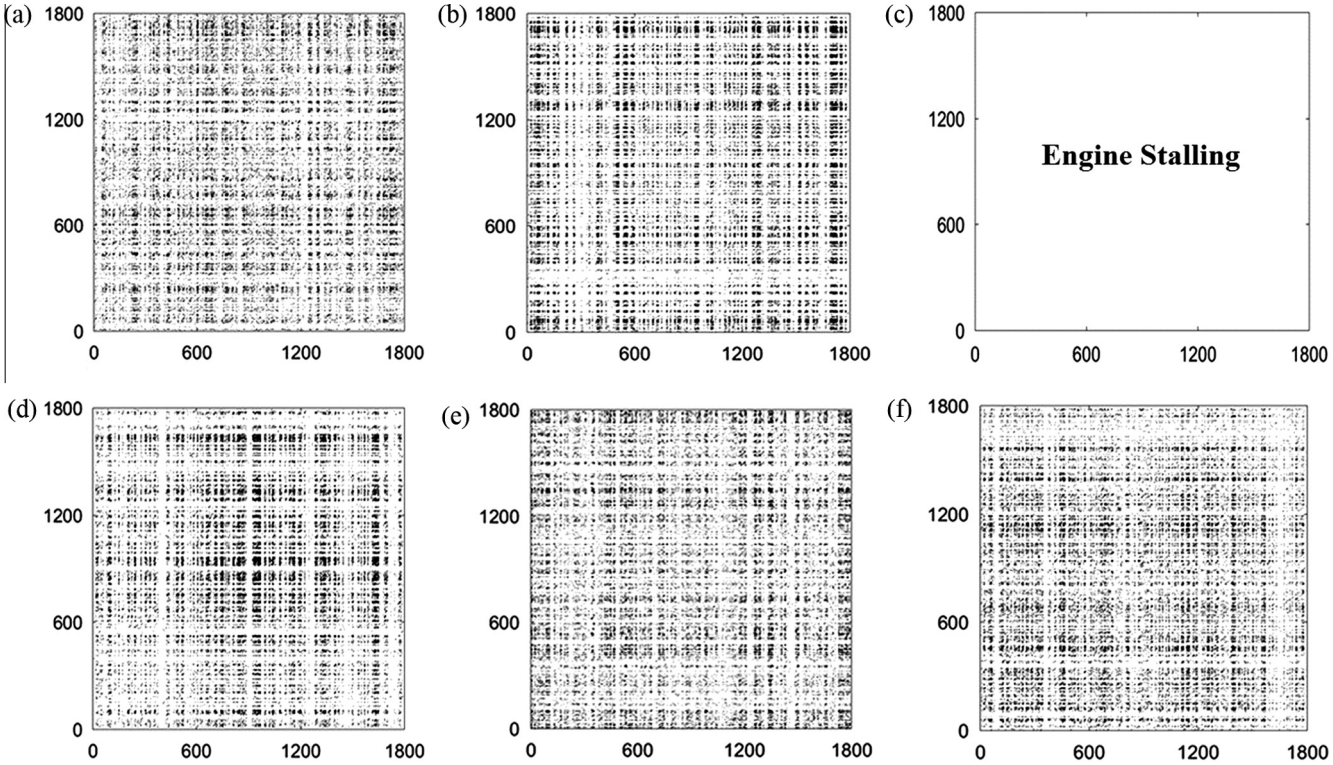

Fig. 12. RPs when λ = 1.6, the engine load is 10% and the engine speed is 1000 rpm: (a–f) correspond to GITs of 1, 30, 60, 90, 120 and 150°CA ATDC.

caused by the effect of gas fuel residual from the prior cycles. In Fig. 15, the position of the ignition kernel of the spark plug was marked by a black dot.

Interestingly, Fig. 15 presents the in-cylinder CH_4 concentration when the piston is located at 2°CA before ignition. The results for GIT of 1°CA ATDC show that the CH_4 concentration is highest in

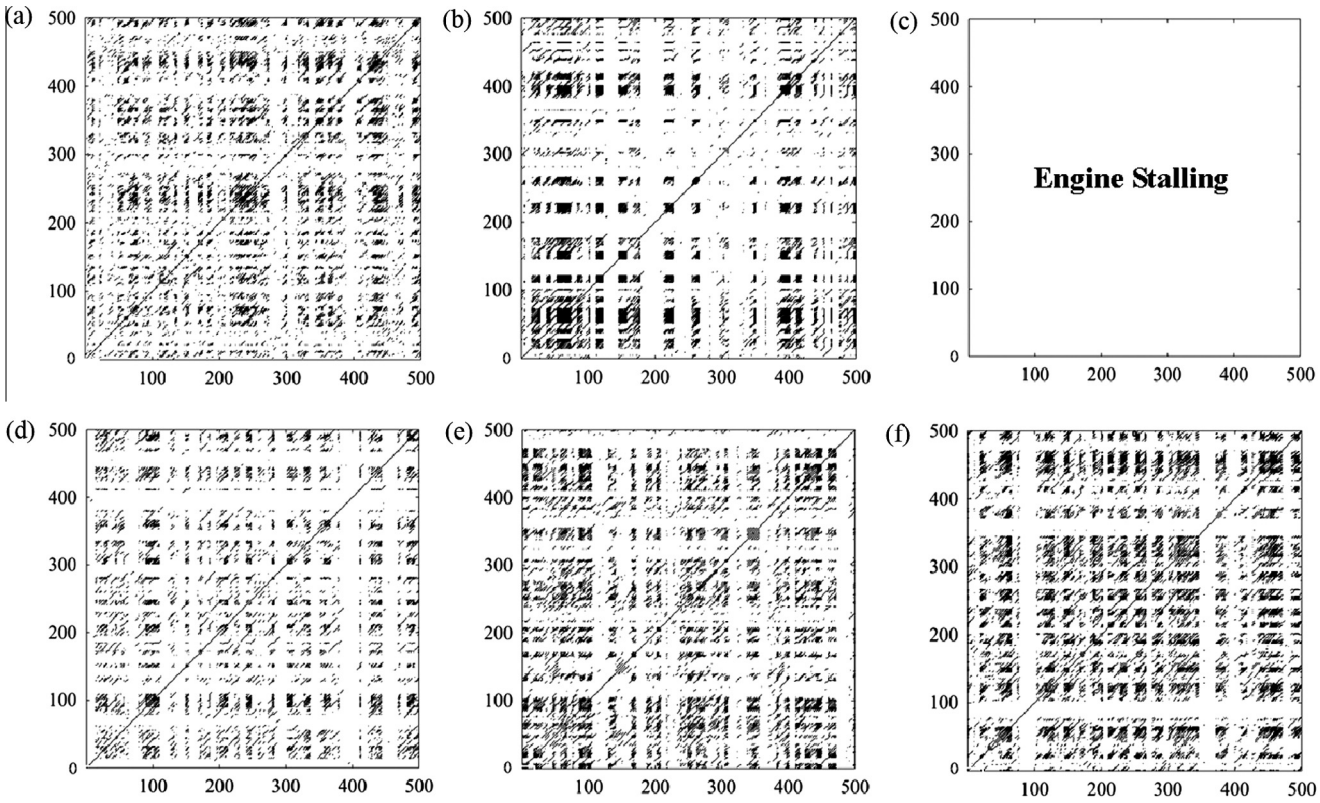

Fig. 13. The small-scale structures of Fig. 12.

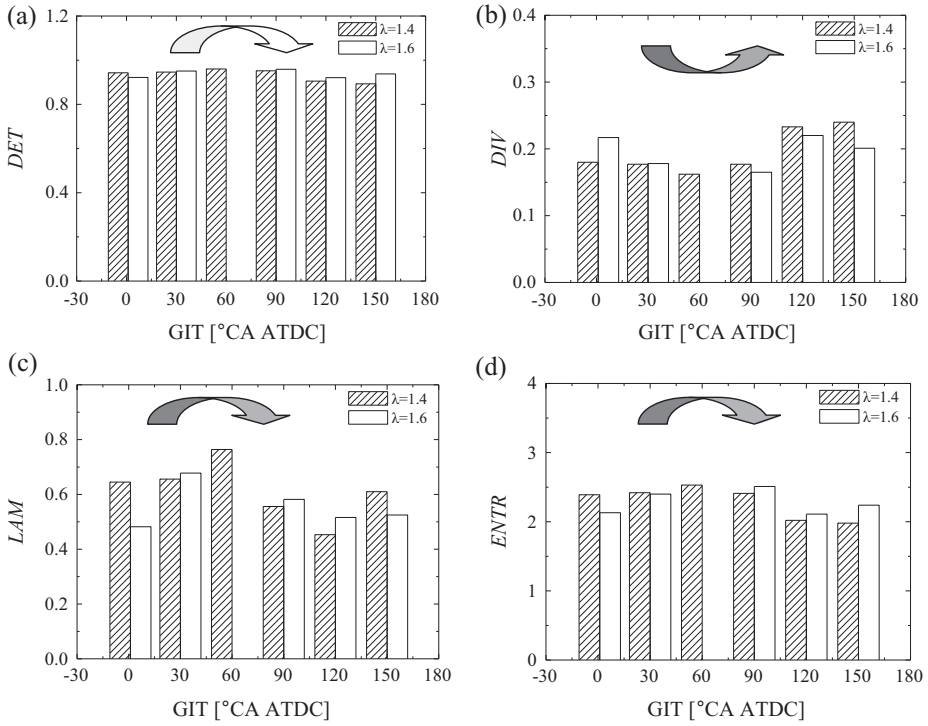

Fig. 14. Comparison of RQA measures when the engine load is 10%, speed is 1000 rpm, λ is1.4 and 1.6 respectively. The RR is the same (RR = 0.1) for all studied engine conditions.

the middle and at the top, and the local mass fraction of CH_4 near the spark plug is approximately 0.038. This value is corresponding to λ of 1.48 and is richer than the average value of λ (1.6). Such stratification of CH_4 concentration is more beneficial to the formation and its development of the initial flame core, which can lead to more stable combustion in lean-burn natural gas engines. As GIT is

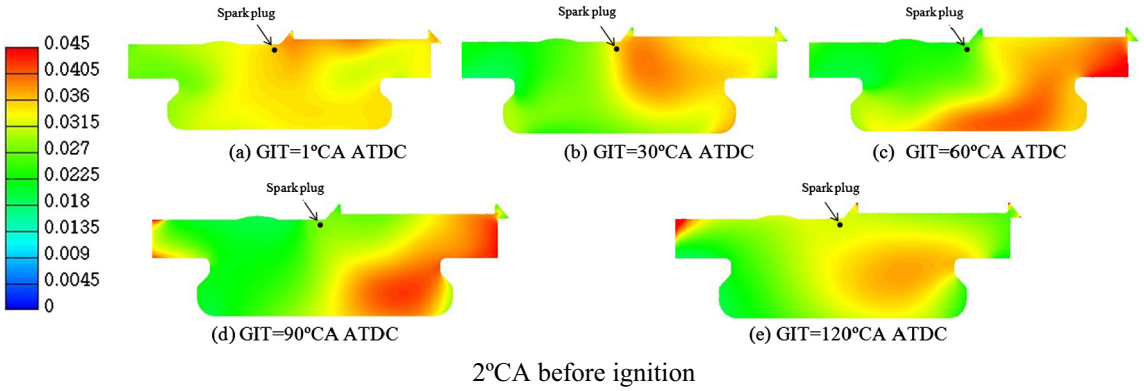

Fig. 15. The distribution of CH_4 concentration in-cylinder when the engine load is 10%, the engine speed is 1000 rpm, λ is 1.6 and GIT is from 1 to 120°CA ATDC.

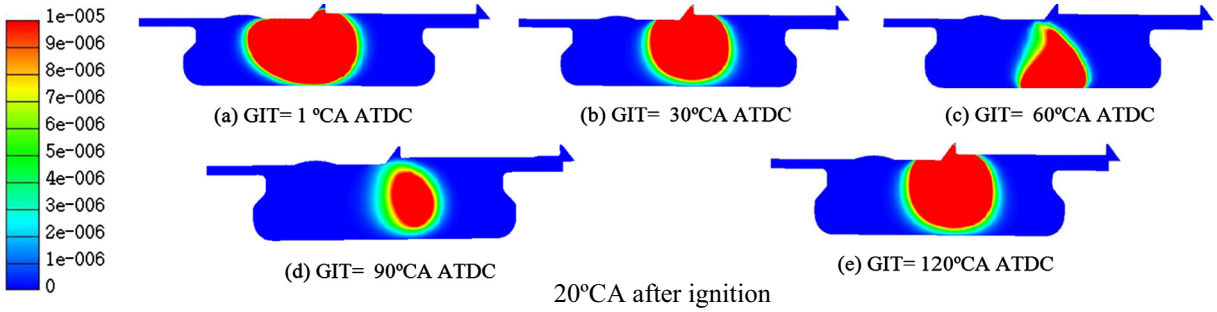

Fig. 16. The distribution of OH concentration in-cylinder when the engine load is 10%, the engine speed is 1000 rpm, λ is 1.6 and GIT is from 1 to 120°CA ATDC.

30°CA ATDC, the CH_4 concentration near the spark plug is higher, but if a small variation of CH_4 distribution (especially for the leaner mixture) caused by turbulent motion of in-cylinder mixture occurs, it will produce an amplified effect on combustion instabilities, the randomness of combustion process increases, and so drastic combustion fluctuations occur (see Fig. 6(b)). However, we can notice from Fig. 15(c) that for GIT of 60°CA ATDC, the CH_4 mass fraction near the spark plug is 0.027 (λ is 2.1). Too lean mixture of CH_4 and air is difficult to ignite, and even though it can be initially oxidised, the flame core cannot be maintained and developed because there is only a small amount of energy input from the surrounding elements. In addition, the turbulence in-cylinder can also increase the probabilities of engine misfire. Therefore, such structure of CH_4 concentration fields results in an increase of the dynamic complexity of combustion system (see Fig. 14). As the GIT increases, although structures of CH4 concentration fields are not so reasonable because the richer mixture is located in the lower right region in the combustion chamber, the local CH_4 concentration near the spark plug gradually increases (see Fig. 15(d) and (e)), leading to more stable combustion of lean-burn natural gas engines. This can be observed in Fig. 6 (e) and (f). From the discussion above, we can clearly identify the source of combustion instabilities and the main reason for the increase in complexity of combustion systems.

Fig. 16 presents the in-cylinder OH concentration distributions at 20°CA after ignition. It is clear that with the increase of GIT, the flame radius decreases first, and then increases. For earlier (GIT < 30°CA ATDC) or delayed (GIT > 90°CA ATDC) gas injection, the relatively reasonable CH_4 concentration distributions near the spark plug before ignition (see Fig. 15(a), (b) and (e)) lead to more stable initial kernel and fast flame propagation, the shapes of flame front face are more regular quasi-elliptic (see Fig. 16(a), (b) and (e)). However, for the intermediate value of GIT, the speed of flame propagation is lower (see Fig. 16(c) and (d)). From the discussion above, it is clear that the combustion instabilities and increasing complexity of pre-mixed lean-burn natural gas engine are from unreasonable stratification of CH_4 concentration.

During the study of control strategy and performance calibration of natural gas engine, usually researchers or engineers may pay more attention to calibrating or optimizing spark ignition timing and air/fuel ratio (by adjusting gas injection pulse width) under different engine operating conditions, at higher engine load, in order to avoid the residual of mixture of air and gas fuel in intake manifold, earlier gas injection should be adopted and there is a small adjustable range of GIT, however our research results show that at low load the gas injection pulse width is very small, so a constant gas injection timing is obviously unreasonable because the combustion instabilities and complexity of combustion system are very sensitive to change of GIT, properly earlier or delayed gas injection will lead to more stable and improved combustion, this means that intermediate values of GIT should be avoided.

5. Conclusions

In this study, the cyclic combustion instabilities of the indicated mean effective pressure (IMEP) in a pre-mixed lean natural gas engine have been investigated when the engine speed was 1000 rpm, the engine load rate was 10%, and λ was 1.4 and 1.6 respectively. For each mixture concentration (λ), the combustion instabilities for six different values of gas injection timing (GIT) were analysed. Using non-linear embedding theory, recurrence plots (RPs), recurrence quantification analysis (RQA), the hidden rhythms and the dynamic complexity of the combustion system have been examined and the possible source of combustion instabilities in a pre-mixed lean-burn natural gas engine has been identified, based on 3-D computational fluid dynamics (CFD) simulation.

(1) Comparing a large engine load and richer mixture, GIT has a more significant effect on combustion instabilities in natural gas engines under lower load and using a leaner mixture, and earlier (GIT < 30°CA ATDC) or delayed (GIT > 90°CA ATDC) gas injection will lead to more stable combustion and higher power output, while the medium GITs (from 30 to 90°CA ATDC) will lead to an increase of combustion fluctuations and poor engine performance.

(2) For richer mixture, earlier or delayed gas injection leads to relatively small and quasi-circular structures of attractors in phase space, and the state points of attractors appear time–reversible, a series of short lines parallel to the main diagonal line in RPs indicate the more regular oscillatory behaviour of the combustion system. However, the medium GITs lead to the increase of randomness of distribution of state points in phase space and the attractors with more loosened and bifurcated geometric structure, and the "characteristic arms" of attractors were clearly observed. While the mixture becomes leaner, the medium GITs result in the increasing asymmetry of attractors and denser "characteristic arms", which exhibit time-irreversibility. The preponderance of vertical or horizontal lines in RPs signifies the presence of laminar states or intermittency in the IMEP time series. The white bands in the RPs may be caused by misfire or partial combustion.

(3) For different mixture concentrations, except for DIV, the other RQA measures exhibit the same variation trends with GIT. With the increase of GIT, the RQA measures first increase, and then decrease. For the leaner mixture and medium GITs, the higher ENTR mean the higher system complexity. The combustion instabilities and increasing complexity are from unreasonable stratification of mixture concentration, unreliable formation of initial ignition core and turbulent motion in-cylinder.

Our research results are useful to understand the inherent nature and complex dynamics of combustion systems, to identify the source of combustion instabilities, and then develop more intelligent control strategies and to further extend the combustion boundary of pre-mixture lean-burn natural gas engines.

Acknowledgments

This work was supported by the National Natural Science Foundation of China (51306041), Natural Science Foundation of Heilongjiang Province of China (QC2013C057).

References

[1] Energy Information Administration. Washington, DC: US Department of Energy; 2002.
[2] Cho HM, He BQ. Spark ignition natural gas engines - a review. Energy Convers Manage 2007;48:608–18. http://dx.doi.org/10.1016/j.enconman.2006.05.023.
[3] Maclean HL, Lave LB. Evaluating automobile fuel/propulsion system technologies. Prog Energy Combust 2003;29:1–69. http://dx.doi.org/10.1016/S0360-1285(02)00032-1.
[4] Kato T, Saeki K, Nishide H, Yamada T. Development of CNG fueled engine with lean-burn for small size commercial van. JSAE Rev 2001;22:365–8. http://dx.doi.org/10.1016/S0389-4304(01) 00104-7.
[5] Roethlisberger RP, Favrat D. Comparison between direct and indirect (prechamber) spark ignition in the case of a cogeneration natural gas engine, Part I: engine geometrical parameters. Appl Therm Eng 2002;22:1217–29. http://dx.doi.org/10.1016/S1359 -4311(02)00040-6.
[6] Peterson MB, Barter GE, West TH, Manley DK. A parametric study of light-duty natural gas vehicle competitiveness in the United States through 2050. Appl Energy 2014;125:206–17. http://dx.doi.org/10.1016/j.apenergy.2014.03.062.
[7] Zhang Q, Li MH, Shao SD. Combustion process and emissions of a heavy-duty engine fueled with directly injected natural gas and pilot diesel. Appl Energy 2015;157:217–28. http://dx.doi.org/10.1016/j.apenergy.2015.08.021.
[8] Ibrahim A, Bari S. A comparison between EGR and lean-burn strategies employed in a natural gas SI engine using a two-zone combustion model. Energy Convers Manage 2009;50:3129–39. http://dx.doi.org/10.1016/j.enconman.2009.08.012.
[9] Lee S, Park S, Kim C, Kim YM, Park C. Comparative study on EGR and lean burn strategies employed in an SI engine fueled by low calorific gas. Appl Energy 2014;129:10–6. http://dx.doi.org/10.1016/j.apenergy.2014.04.082.
[10] Hajbabaei M, Karavalakis G, Johnson KC, Lee L, Durbin TD. Impact of natural gas fuel composition on criteria, toxic, and particle emissions from transit buses equipped with lean burn and stoichiometric engines. Energy 2013;62:425–34. http://dx.doi.org/10.1016/j.energy.2013.09.040.
[11] Morteza F, Khoshbakhti SR, David CM. The influence of exhaust gas recirculation (EGR) on combustion and emissions of *n*-heptane/natural gas fueled homogeneous charge compression ignition (HCCI) engines. Appl Energy 2011;88:4719–24. http://dx.doi.org/10.1016/j.apenergy.2011.06.017.
[12] Das A, Watson HC. Development of a natural gas spark ignition engine for optimum performance. J Automob Eng 1997;211:361–78.
[13] Lumsden G, Eddleston D, Sykes R. Comparing lean-burn and EGR. SAE paper, no. 970505; 1997. http://dx.doi.org/10.4271/970505.
[14] Cho HM, He BQ. Spark ignition natural gas engines - a review. Energy Convers Manage 2007;48:608–18. http://dx.doi.org/10.1016/j.enconman.2006.05.023.
[15] Maurya RK, Agarwal AK. Experimental investigation on the effect of intake air temperature and air–fuel ratio on cycle-to-cycle variations of HCCI combustion and performance parameters. Appl Energy 2011;88:1153–63. http://dx.doi.org/10.1016/j.apenergy.2010.09.027.
[16] Ozdor N, Dulger M, Sher E. Cyclic variability in spark ignition engines: a literature survey. SAE paper, no. 940987; 1994. http://dx.doi.org/10.4271/940987.
[17] Reyes M, Tinaut FV, Giménez B, Pérez A. Characterization of cycle-to-cycle variations in a natural gas spark ignition engine. Fuel 2015;140:752–61. http://dx.doi.org/10.1016/j.fuel.2014.09.121.
[18] Navarroa E, Leo TJ, Corral R. CO_2 emissions from a spark ignition engine operating on natural gas–hydrogen blends (HCNG). Appl Energy 2013;101:112–20. http://dx.doi.org/10.1016/j.apenergy.2012.02.046.
[19] Evans RL. Extending the lean limit of natural-gas engines. J Eng Gas Turb Power 2009;131:032803. http://dx.doi.org/10.1115/1.3043814.
[20] He ZY, Jing QJ, Zhu L, Zhang WG, Huang Z. The effects of different intake charge diluents on the combustion and emission characteristics of a spark ignition natural gas engine. Appl Therm Eng 2015;89:958–67. http://dx.doi.org/10.1016/j. applthermaleng.2015.06.072.
[21] Zhang HG, Han XJ, Yao BF, Li GX. Study on the effect of engine operation parameters on cyclic combustion variations and correlation coefficient between the pressure-related parameters of a CNG engine. Appl Energy 2013;104:992–1002. http://dx.doi.org/10.1016/j.apenergy.2012.11.043.
[22] Wagner RM, Drallmeier JA, Daw CS. Characterization of lean combustion instability in pre-mixed charge spark ignition engines. Int J Engine Res 2001;1:301–20. http://dx.doi.org/10.1243/1468087001545209.
[23] Kamiński T, Wendeker M, Urbanowicz K, Litak G. Combustion process in a spark ignition engine: dynamics and noise level estimation. Chaos 2004;14:461–6. http://dx.doi.org/10.1063/1.1739011.
[24] Maurya RK, Agarwal AK. Experimental investigation of cyclic variations in HCCI combustion parameters for gasoline like fuels using statistical methods. Appl Energy 2013;111:310–23. http://dx.doi.org/10.1016/j.apenergy.2013.05.004.
[25] Wendeker M, Czarnigowski J, Litak G, Szabelski K. Chaotic combustion in spark ignition engines. Chaos Soliton Fract 2003;18:803–6. http://dx.doi.org/10.1016/S0960-0779(03)00031-6.
[26] Kyrtatos P, Brückner C, Boulouchos K. Cycle-to-cycle variations in diesel engines. Appl Energy 2016;171:120–32. http://dx.doi.org/10.1016/j.apenergy.2016.03.015.
[27] Sen AK, Litak G, Yao BF, Li GX. Analysis of pressure fluctuations in a natural gas engine under lean burn conditions. Appl Therm Eng 2010;30:776–9. http://dx.doi.org/10.1016/j.applthermaleng.2009.11.002.
[28] Li GX, Yao BF. Nonlinear dynamics of cycle-to-cycle combustion variations in a lean-burn natural gas engine. Appl Therm Eng 2008;28:611–20. http://dx.doi.org/10.1016/j.applthermaleng.2007.04.008.
[29] Wang LY, Yang LP, Jing HG, Qaisar H, Liu GD. Effect of spark condition on nonlinear dynamic characteristics of natural gas engine. AASRI Proc 2012;1:150–5.
[30] Barton RK, Kenemuth DK, Lestz SS, Meyer WE. Cycle-by-cycle variations of a spark ignition engine - a statistical analysis. SAE paper, no. 700488; 1970. http://dx.doi.org/10.4271/700488.
[31] Martin JK, Plee SL, Remboski DJ. Burn modes and prior-cycle effects on cyclic variations in lean-burn spark-ignition engine combustion. SAE paper, no. 880201; 1988. http://dx.doi.org/10.4271/880201.
[32] Moriyoshi Y, Kanimoto T, Yagita M. Prediction of cycle-to-cycle variation of in-cylinder flow in a motored engine. SAE paper, no. 930066; 1993. http://dx.doi.org/10.4271/930066.
[33] Daily J. Cycle-to-cycle variations: a chaotic process? SAE paper, no. 870165; 1987. http://dx.doi.org/10.4271/870165.
[34] Litak G, Taccani R, Radu R, Urbanowicz K, et al. Estimation of a noise level using coarse-grained entropy of experimental time series of internal pressure in a combustion engine. Chaos Soliton Fract 2005;23:1695–701. http://dx.doi.org/10.1016/j.chaos.2004.06.057.
[35] Curto-Risso PL, Medinab A, Hernández AC, et al. On cycle-to-cycle heat release variations in a simulated spark ignition heat engine. Appl Energy 2011;88:1557–67. http://dx.doi.org/10.1016/j.apenergy.2010.11.030.
[36] Wagner RM, Drallmeier J, Daw CS. Prior-cycle effects in lean spark ignition combustion - fuel/air charge considerations. SAE paper, no. 981047; 1998. http://dx.doi.org/10.4271/981047.

[37] Daw CS, Finney CEA, Green JB, et al. A simple model for cyclic variations in a spark-ignition engine. SAE paper, no. 962086; 1996. http://dx.doi.org/10.4271/962086.
[38] Sen AK, Litak G, Kaminski T, Wendeker M. Multifractal and statistical analyses of heat release fluctuations in a spark ignition engine. Chaos 2008;18:033115. http://dx.doi.org/10.1063/1.2965502.
[39] Sen AK, Wang JH, Huang ZH. Investigating the effect of hydrogen addition on cyclic variability in a natural gas spark ignition engine: wavelet multiresolution analysis. Appl Energy 2011;88:4860–6. http://dx.doi.org/10.1016/j.apenergy.2011.06.030.
[40] Sen AK, Zheng JJ, Huang ZH. Dynamics of cycle-to-cycle variations in natural gas direct-injection spark-ignition. Appl Energy 2011;88:2324–34. http://dx.doi.org/10.1016/j.apenergy.2011.01.009.
[41] Sen AK, Ash SK, Huang B, Huang ZH. Effect of exhaust gas recirculation on the cycle-to-cycle variations in a natural gas spark ignition engine. Appl Therm Eng 2011;31:2247–53. http://dx.doi.org/10.1016/j.applthermaleng.2011.03.018.
[42] Litak G, Syta A, Yao BF, Li GX. Indicated mean effective pressure oscillations in a natural gas combustion engine by recurrence plots. J Theor Appl Mech-Pol 2009;47:55–67.
[43] Litak G, Kaminski T, Rusinek R, Czarnigowski J, Wendeker M. Patterns in the combustion process in a spark ignition engine. Chaos Soliton Fract 2008;35:578–85. http://dx.doi.org/10.1016/j.chaos.2006.05.053.
[44] Yang LP, Ding SL, Litak G, Song EZ, Ma XZ. Identification and quantification analysis of non-linear dynamics properties of combustion instability in a diesel engine. Chaos 2015;25:013105. http://dx.doi.org/10.1063/1.4899056.
[45] Eckmann JP, Kamphorst SO, Ruelle D. Recurrence plots of dynamical systems. EPL-Europhys. Lett. 1987;4:973–7.
[46] Zbilut JP, Webber CL. Embeddings and delays as derived from quantification of recurrence plots. Phys Lett A 1992;171:199–203. http://dx.doi.org/10.1016/0375-9601(92)90426-M.
[47] Webber CL, Zbilut JP. Dynamical assessment of physiological systems and states using recurrence plot strategies. J Appl Physiol 1994;76:965–73.
[48] Marwan N. How to avoid potential pitfalls in recurrence plot based data analysis. Int J Bifurcat Chaos 2011;21:1003–17. http://dx.doi.org/10.1142/S0218127411029008.
[49] Marwan N, Romano MC, Thiel M, Kurths J. Recurrence plots for the analysis of complex systems. Phys Rep 2007;438:237–329. http://dx.doi.org/10.1016/j.physrep.2006.11.001.
[50] Marwan N, Wessel N, Meyerfeldt U, Schirdewan A, Kurths J. Recurrence plot based measures of complexity and its application to heart rate variability data. Phys Rev E 2002;66:026702. http://dx.doi.org/10.1103/PhysRevE.66.026702.
[51] Marwan N. Recurrence plots tool. http://tocsy.pik-potsdam.de/CRPtoolbox/.
[52] Heywood JB. Internal combustion engine fundamentals. New York: McGraw-Hill; 1988.
[53] Zeng K, Huang ZH, Liu B, et al. Combustion characteristics of a direct-injection natural gas engine under various fuel injection timings. Appl Therm Eng 2006;26:806–13. http://dx.doi.org/10.1016/j.applthermaleng.2005.10.011.
[54] Baratta M, Rapetto N. Mixture formation analysis in direct-injection NG SI engine under different injection timings. Fuel 2015;159:675–88. http://dx.doi.org/10.1016/j.fuel.2015.07.027.
[55] Hiltner J, Samimy M. The impact of injection timing on in-cylinder fuel distribution in a natural gas powered engine. SAE paper, no. 971708; 1997. http://dx.doi.org/10.4271/971708.
[56] Yamato T, Hayashida M, Sekino H, Sugahara K. Effect of injection timing on the performance of a manifold injection gas engin. SAE paper, no. 1999-01-3295; 1999. http://dx.doi.org/10.4271/1999-01-3295.
[57] Yang B, Xi CG, Wei X, et al. Parametric investigation of natural gas port injection and diesel pilot injection on the combustion and emissions of a turbocharged common rail dual-fuel engine at low load. Appl Energy 2015;143:130–7. http://dx.doi.org/10.1016/j.apenergy.2015.01.037.
[58] Abarbanel HDI. Analysis of observed chaotic data. New York: Springer-Verlag; 1996.
[59] Kennel MB, Brown R, Abarbanel HDI. Determining embedding dimension for phase-space reconstruction using a geometrical construction. Phys Rev A 1992;45:3403. http://dx.doi.org/10.1103/PhysRevA.45.3403.
[60] Green JB, Daw CS, Armfield JS, et al. Time irreversibility and comparison of cyclic-variability models. SAE paper, no. 1999-03-01; 1999. http://dx.doi.org/10.4271/1999-01-0221.